ANNALI DI GEOFISICA, VOL. XXXVII, N. 6, December 1994

Focal mechanism determination for volcanic microearthquakes

Giuseppe De Natale
Osservatorio Vesuviano, Napoli, Italy

Abstract
Classical methods to infer focal mechanisms from first *P* wave motions are of limited use for the analysis of small magnitude events occurring in volcanic areas, due to structure complexity. This work presents an alternative way to compute focal mechanisms of earthquakes in volcanic areas, based on a Bayesian approach. The probability density on the whole space spanned by source parameters is graphically represented, by a method originally due to Bernard and Zollo (1989). The data used to infer the probability density function can be of various kinds, like *P* wave polarities, *S* wave polarizations and *S/P* direct wave amplitude ratios. *S* wave polarizations are left practically unchanged by smooth variations of velocity, and are only sensitive to strong discontinuities and/or seismic anisotropy. *S/P* amplitude ratios of direct waves are also good observables, not very sensitive to frequency independent amplification effects. They are still affected by differential *S-P* anelastic attenuation, although to a much lesser extent than absolute *S* and *P* amplitudes. In fact, the use of complete waveforms is not desiderable in volcanic areas because wave amplitudes may be strongly biased by not well known path and site effects, mainly for non direct waves which are most affected by medium heterogeneities. Such unmodeled elastic and anelastic features of the medium can be traded off for source characteristics, leading to bad results. The use of the probabilistic approach, and the selection of robust observables, allow us to solve many problems of classical methods. The determination of the whole probability density on the parameter space visualizes all the information contained in the data set, checking completely the goodness of the solution, and its univoqueness. Furthermore, the use of different kinds of robust data sets helps to constrain the solution, and to minimize the influence of unmodeled medium heterogeneities. In the present method, it is possible to parameterize the source in terms of both double couple sources, and other kinds of sources generally hypothesized on volcanoes (tensile crack, CLVD, explosion) or generic sources characterized by five normalized independent components of the moment tensor. *S/P* amplitude ratios are shown to be those which most constrain the source mechanism. Furthermore, this paper analyzes the influence of anelastic attenuation on *S* and *P* absolute amplitudes, and on *S/P* amplitude ratios. An example of application to a small (M_L = 2.0) earthquake which occurred at Campi Flegrei caldera is reported, showing how the different data sets constrain the solution. Finally, an example is reported of extensive application of the method to the analysis of small earthquakes which occurred at Campi Flegrei (Southern Italy) caldera during an unrest episode (1982-1984). It is shown how the accurate analysis of small earthquakes within a caldera has helped to solve important volcanological questions like: the caldera structure, the mechanism of earthquake generation during unrest episodes, and the features of ground deformations in calderas.

Key words *volcanic microearthquakes – focal mechanisms – Bayesian estimation*

1. Introduction

The reliable estimation of focal mechanisms for small to moderate sized earthquakes is generally a difficult task. This is mainly due to the limited amount of data available for small magnitude events. Moreover, large errors in the computed fault plane parameters are related to the uncertainties of the earthquake location and the assumed Earth velocity model. In fact, in case of small source-receiver distances (as for microearthquake studies), even small changes in the event location or in the structure parameters may produce large variations in the

P and S ray take-off angles at the source. In addition, the routine methods which compute the fault plane solutions from a set of P-onset polarity readings, are not well suited to handling the general non-linear inverse problem of fault mechanism determination. The non-linearity generally arises from a poor azimuth and distance coverage of the source and the uncertainty of the assumed velocity model. Focal mechanism determination for earthquakes occurring in volcanic areas is further complicated by the possibility of having mechanisms different from the double couple (CLVD, tensile cracks, etc.). The use of wave amplitudes can strongly constrain focal mechanism solutions for small earthquakes, but they are not «robust» observables, because they are very sensitive to propagation effects. De Natale *et al.* (1987) and De Natale and Zollo (1989) developed an inverse method to determine the focal mechanisms of small earthquakes by inversion of P and S direct pulse amplitudes. Sileny *et al.* (1992) developed a method based on complete waveform modeling. In any case, anelastic attenuation can seriously affect P and S wave amplitudes, particularly in volcanic areas, making it very difficult to compute a reliable solution. The present paper presents a general approach to compute focal mechanisms of earthquakes in volcanic areas. The method is based on the probabilistic approach by Zollo and Bernard (1991) and De Natale *et al.* (1991), which can be easily generalized to compute mechanisms different from the double couple. In the framework of this method, only robust observables, *i.e.* not very sensitive to propagation effects, are used to determine focal mechanisms. In addition to P wave polarity data, direct S wave polarization directions and S/P amplitude ratios, strongly constraining mechanisms are used. In particular, S/P amplitude ratios are the most constraining on the kind of mechanism (double couple, tensile crack, etc.). The influence of anelastic attenuation on absolute amplitudes and on S/P amplitude ratios is discussed. An application of the method to the computation of double couple focal mechanisms at the Campi Flegrei (Italy) volcanic area is also shown, following the results obtained by De Natale *et al.* (1993).

2. Direct method for amplitude determinations

In order to generate theoretical S wave polarizations and S/P amplitude ratio, we need to compute P, SV and SH amplitudes as a function of the fault parameters, specifying the mechanism at the source.

When interested in studying earthquakes occurring in volcanic areas, one should consider, in addition to the double couple, other kinds of source mechanisms. In this paper, I further consider the modeling of tensile crack and compensated linear vector dipole (CLVD, Knopoff and Randall, 1970) mechanisms.

For each kind of mechanism, a set of source parameters is specified, allowing synthetic amplitudes of body waves to be computed. The basic formulas to compute far-field wave amplitudes generated by a generic moment tensor M are given by Aki and Richards (1980):

$$\boldsymbol{u}^{P}(\boldsymbol{x}, t) = \frac{\gamma \dot{M}(t - \tau_{\alpha})\gamma}{4\pi\rho^{1/2}(\boldsymbol{x})\rho^{1/2}(\xi)\alpha^{5/2}(\xi)\alpha^{1/2}(\boldsymbol{x})R(\boldsymbol{x}, \xi)}\boldsymbol{l}$$

$$\boldsymbol{u}^{SV}(\boldsymbol{x}, t) = \frac{\boldsymbol{p}\,\dot{M}(t - \tau_{\beta})\gamma}{4\pi\rho^{1/2}(\boldsymbol{x})\rho^{1/2}(\xi)\beta^{5/2}(\xi)\beta^{1/2}(\boldsymbol{x})R(\boldsymbol{x}, \xi)}\boldsymbol{p}$$

$$\boldsymbol{u}^{SH}(\boldsymbol{x}, t) = \frac{\phi\,\dot{M}(t - \tau_{\beta})\gamma}{4\pi\rho^{1/2}(\boldsymbol{x})\rho^{1/2}(\xi)\beta^{5/2}(\xi)\beta^{1/2}(\boldsymbol{x})R(\boldsymbol{x}, \xi)}\phi$$

where the unit vectors $\boldsymbol{l}$, $\boldsymbol{p}$ and ϕ give the directions of radial and transverse motions at the receiver respectively, and γ is the unit vector giving the direction of the take-off angle at the source, as shown in fig. 1. $R(\boldsymbol{x}, \xi)$ is the geometrical spreading, which depends on the characteristics of the propagation medium; $\tau_{\alpha,\beta}$ is the time for propagation of the considered wave (P or S) from the source ξ to the receiver $\boldsymbol{x}$; α, β, ρ are P, S wave velocities and density, respectively.

If the moment tensor is time independent, $\dot{M}(t) = M_{\phi}\,\dot{s}(t)$, where $\dot{s}(t)$ is the source time function. Thus, given the moment tensor components, maximum wave amplitudes (*i.e.*, the maximum of the function $M_{\phi}\,\dot{s}(t)$) can be computed.

Using the diagonal form of M_{ϕ} in the princi-

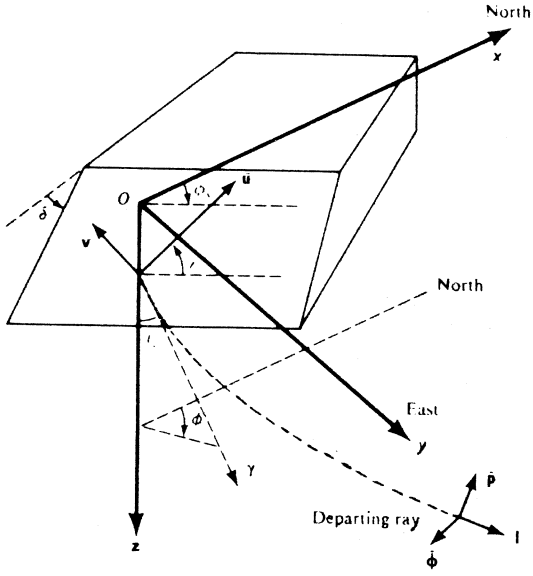

Fig. 1. Geometry of the seismic ray and fault parameters (Aki and Richards, 1980).

pal system, depending on the kinds of mechanisms considered, formulas can be written as a function of the fault parameters, specified as follows (Aki and Richards, 1980):
double couple: fault strike (ϕ), dip (δ) and slip (λ);
tensile crack: fault strike (ϕ), dip (δ);
CLVD: fault strike (ϕ), dip (δ).

The geometry of the double couple solution is completely specified by three parameters, whereas only two parameters characterize tensile crack and CLVD. Such difference in the number of free parameters of the three source models must be carefully considered when trying to discriminate the source mechanism on the basis of the fit to the data. In fact, models with more free parameters always give a best fit, but the improvement with respect to simpler models may be not statistically significant.

3. Effect of attenuation on wave amplitudes

The effect of attenuation in volcanic areas can be particularly marked, because in such areas low Q values, between 10 and 100, are common. The effect of low Q values can significantly bias estimates of wave amplitudes, and hence focal mechanisms computed by such observables. Using the Carpenter (1966) operator for anelastic attenuation, the influence on P and S pulses (modeled as Hanning's pulses) has been computed, for characteristic frequencies of 2, 5 and 10 Hz, and distances of 5 and 10 km. Table I shows the

Table I. Attenuation factors for displacement (d) and velocity (v) pulses (Hanning's pulses and first derivatives).

	P waves					S waves			
	f_c = 2 Hz	f_c = 5 Hz	f_c = 10 Hz			f_c = 2 Hz	f_c = 5 Hz	f_c = 10 Hz	
				Q = 50					
R = 5 km	0.89	0.75	0.57	d	R = 5 km	0.81	0.62	0.41	d
	0.83	0.65	0.45	v		0.73	0.49	0.27	v
R = 10 km	0.79	0.58	0.37	d	R = 10 km	0.67	0.42	0.24	d
	0.70	0.45	0.24	v		0.55	0.27	0.11	v
				Q = 100					
R = 5 km	0.94	0.86	0.74	d	R = 5 km	0.90	0.78	0.61	d
	0.90	0.80	0.65	v		0.86	0.68	0.49	v
R = 10 km	0.89	0.75	0.57	d	R = 10 km	0.81	0.62	0.41	d
	0.82	0.65	0.45	v		0.73	0.49	0.27	v

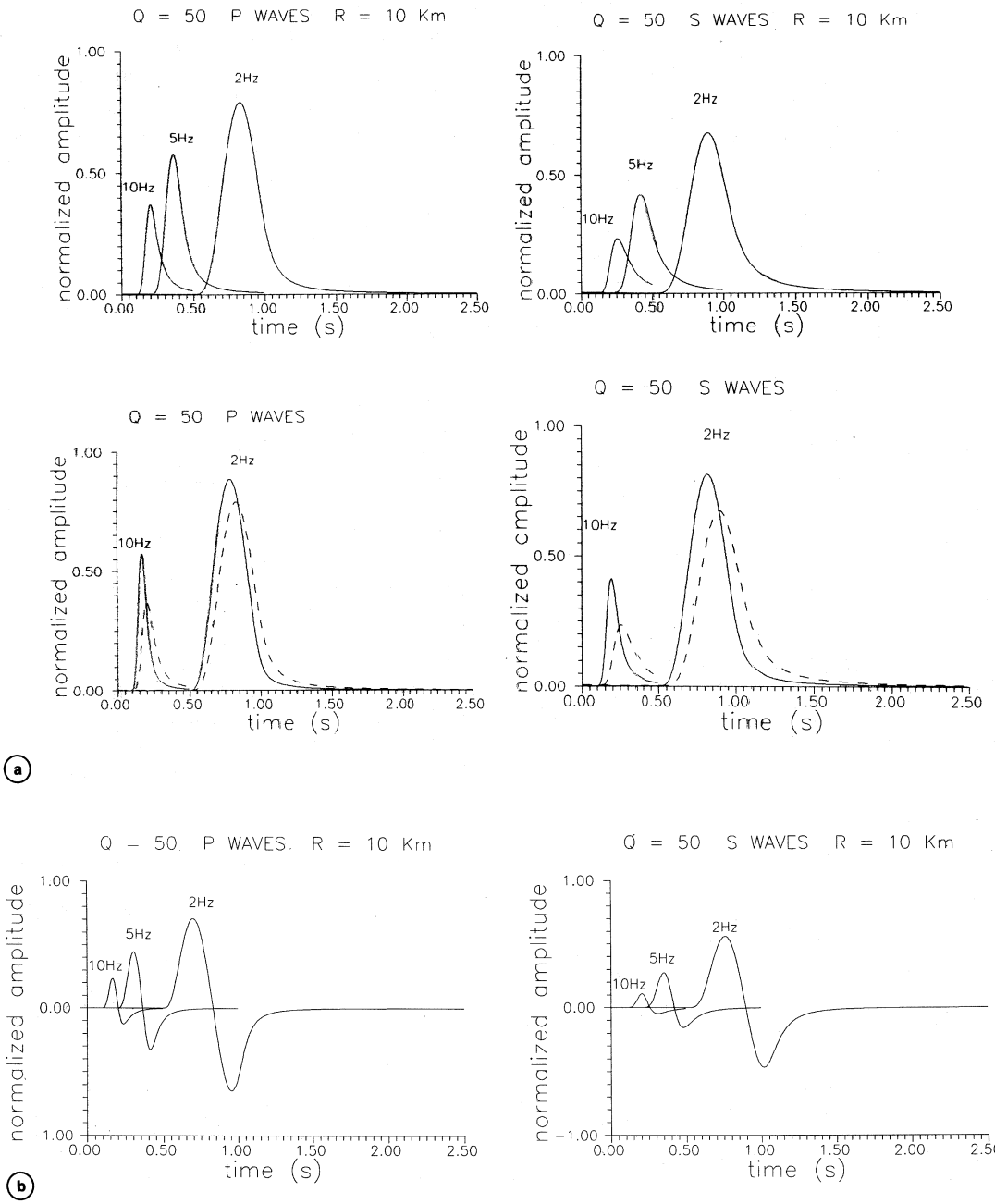

Fig. 2a,b. Examples of attenuated Hanning's pulses (simulating seismic displacements) and time derivatives (seismic velocities) of unit amplitude, by the Carpenter (1966) attenuation operator: a) for displacement; b) for velocity. Solid and dashed lines in (a) indicate respectively distance $R = 5$ km and $R = 10$ km. Wave velocities are $v_p = 3.0$ km/s, $v_s = 1.73$ km/s.

resulting attenuation factors of maximum amplitude, both in displacement and in velocity. Figure 2a,b displays some examples of displacement and velocity pulses, before and after the application of the attenuation operator. As it can be seen, the attenuation of peak amplitude may attain values of one order of magnitude. Such attenuation, if not taken carefully into account, may led to misleading results on focal mechanism determination. Also if the Q value for P and S waves is the same, the attenuation for S waves is larger than for P wave, because S wave is slower than P. Table II reports S/P amplitude ratio attenuation factors. As is clear, the effect on S/P relative amplitudes is lower than the effect on absolute amplitudes, but can still be important. When wave amplitudes are used to discriminate the kind of source mechanism, the effect of anelastic attenuation, if not taken precisely into account, can significantly bias the results. In fact, absolute amplitudes are attenuated in a different way depending on the hypocenter-receiver distance, and hence on azimuth and take-off angles. In addition, the most discriminating observable on the kind of mechanism, as will be shown in the following sessions, is the relative S/P amplitude. Thus, given the linear relationship between the eigenvalues of the moment tensor and the direct wave amplitudes, a decrease in the S/P ratio is reported as an increase of the isotropic component in the source mechanism at the same level. For instance, a 30% of non modeled attenuation in the S/P amplitude ratio, would artificially introduce a 30% increase in the isotropic component of the estimated moment tensor.

Table II. Attenuation factors for S/P amplitude ratios in displacement (d) and velocity (v).

	f_c = 2 Hz	f_c = 5 Hz	f_c = 10 Hz	
		Q = 50		
R = 5 km	0.91	0.83	0.72	d
	0.88	0.75	0.60	v
R = 10 km	0.85	0.72	0.65	d
	0.79	0.60	0.45	v
		Q = 100		
R = 5 km	0.96	0.91	0.82	d
	0.96	0.85	0.75	v
R = 10 km	0.91	0.83	0.72	d
	0.89	0.75	0.60	v

4. Method for focal mechanism determination

The complete description of the applied method can be found in De Natale *et al.* (1991) and Zollo and Bernard (1991). In the following I shall briefly outline the method. It is based on Bayes' rule which provides a quantitative way to incorporate the *a priori* information on the model space and to compute the *a posteriori* probability density function (pdf) $P(\boldsymbol{m} \mid \boldsymbol{d})$ on model parameter vector $\boldsymbol{m}$:

$$P(\boldsymbol{m} \mid \boldsymbol{d}) = \text{const}\, P(\boldsymbol{d}_1 \mid \boldsymbol{m})\, P_0(\boldsymbol{m})\, \mu(\boldsymbol{m}) \qquad (4.1)$$

where: $\boldsymbol{d}$ is the data vector, $P_0(\boldsymbol{m})$ is the *a priori* pdf related to other independent data sets. $P(\boldsymbol{d}_1 \mid \boldsymbol{m})$ is the conditional pdf of one of the considered data sets, for instance the measured S-wave vector directions, $\boldsymbol{d}_1 = (p_1, \ldots, p_{N1})$, ($N_1$ is the number of observations) given a model parameter vector $\boldsymbol{m}$. $\mu(\boldsymbol{m}) = \mu_0(\boldsymbol{m})\, d\boldsymbol{m}$ is denoted, according to Tarantola and Valette (1982) as the «null information» ($\mu_0(\boldsymbol{m})$ is the non-informative pdf). The «null information» represents the state of total ignorance on the model parameters giving equal probability to equal volumes in the parameter space. For the fault mechanism parameter space (parameters are the fault parameters: strike (ϕ) and dip (δ) for tensile crack and CLVD sources, and strike, dip and slip (λ) for double couples) Zollo and Bernard (1991) showed that $\mu_0 = \text{const} \cdot \sin \delta$.

For a given set of S polarization data we can use the Bayes theorem to evaluate the *a posteriori* pdf on model parameters $\boldsymbol{m}$ and use the information inferred from independent data (P-polarities and/or S-to-P amplitude ratios) as *a priori* information represented by an appropriate *a priori* pdf.

We use the following expression for $P(\boldsymbol{d}_1 \mid \boldsymbol{m})$:

$$P(\boldsymbol{d}_1 \mid \boldsymbol{m}) = \prod_{i=1}^{N_1} P(S_i \mid \boldsymbol{m}) \propto$$

$$\propto \exp\left[-\sum_{i=1}^{N_1}(s_i - s_i')^2\ \omega_i^2/\sigma_0^2\right] \times \Theta(\boldsymbol{m}) \tag{4.2}$$

where $(s_i - s_i')$ is the angular difference between the observed and theoretical S vector at station i, ω_i is a weighting factor related to the polarization stability with time. σ_0^2 is the variance, which accounts for errors in the modeling and in the data.

The function $\Theta(\boldsymbol{m})$ is defined as:

$$\Theta(\boldsymbol{m}) = \prod_{i=1}^{N_1} \text{erf}\ (|\, k_s\, R_i^S\,|) \tag{4.3}$$

R_i^S is the theoretical S wave amplitude and k_s is the parameter which controls the amplitude range significantly affected by the error function erf(). This function assigns a low probability to fault models which predict small amplitude S waves at the observation points. The use of function Θ was proposed by De Natale *et al.* (1991) to account for the noise level on S wave records, which make it unlikely to observe very low amplitude signals emitted by earthquakes at the earth's surface.

The additional information on the fault mechanisms carried by P-polarities and S/P amplitude ratios is taken into account by expressing it in the form of an *a priori* pdf. It is implicitly assumed that the different data sets are independent.

Brillinger *et al.* (1980) defined the conditional pdf for a model $\boldsymbol{m}$ given a set of N_2 P-polarity readings:

$$P(\boldsymbol{d}_2 \mid \boldsymbol{m}) \propto \prod_{i=1}^{N_2} 1/2\,[1 + \Psi(R_i^P,\ \gamma_i,\ \rho_i)]\,\rho_i \tag{4.4}$$

where $\Psi = (1 - 2\gamma_i)$ erf($r_i\, R_i^P$) and erf() is the error function.

The quantity in square brackets gives the probability that the observed i-th polarity is coherent with the one computed using the model $\boldsymbol{m}$. R_i^P is the theoretical P amplitude at station i for a given double-couple fault model. γ_i and ρ_i are the parameters which control the shape of the pdf (4.4). These parameters account for the error in ray modeling and the uncertainty on polarity readings due to the noise level (Brillinger *et al.*, 1980). In particular, γ_i represents a tolerance level for polarity violations far from the nodal planes; if $\gamma_i = 0$, the probability of models giving a wrong polarity far from the nodal planes at the i-th station is zeroed.

For N_3 amplitude ratios S/P (denoted by ρ_i), the probability density is defined by the product:

$$P(\boldsymbol{d}_3 \mid \boldsymbol{m}) = \prod_{i=1}^{N_3} P(r_i \mid \boldsymbol{m}) \propto$$

$$\propto \prod_{i=1}^{N_3} F(r_i,\ r_i',\ a_i,\ \tau_i)\ \Theta(\boldsymbol{m}) \tag{4.5}$$

with: $F(x, y, z, t) = 1$ if $|\, x - y\,| < z$

and $F(x, y, z, t) = \exp\ [-(|\, x - y\,| - z)^2/2t^2]$ otherwise.

Practically, when the difference between the observed value r_i and the theoretical one, r_i', is greater than a threshold a_i, the probability density decays with a gaussian profile; when the difference is lower than the threshold, the probability density is constant, and equal to 1. Such shape for the probability density function robustly handles large uncertainties in the S/P amplitude ratios, mainly due to differential attenuation effects between P and S waves, as previously described. In fact, the flat part gives equal weight to the observables within a specified range, conditioned by the uncertainty in attenuation and site effects, whereas the gaussian decay out of the range takes into account

random errors on the amplitudes due, for instance, to the noise on seismograms.

The function:

$$\Theta(\boldsymbol{m}) = \prod_{i=1}^{N_3} \operatorname{erf}(|k_S R_i^S|) \operatorname{erf}(|k_r r_i|) \qquad (4.6)$$

is composed of two terms, the first of which has the effect already explained for *S* polarizations; the second assigns low probability to source models giving small *S/P* amplitude ratios, that would be hardly noted on seismograms, due to the presence of later *P* waves.

The *a priori* probability $P_0(m)$, in the framework of this formulation, is then expressed as:

$$P_0(\boldsymbol{m}) = P(\boldsymbol{d}_2 \mid \boldsymbol{m})\, P(\boldsymbol{d}_3 \mid \boldsymbol{m}) \qquad (4.7)$$

For a given set of *S*-vector directions, *P*-polarity readings and *S/P* amplitude ratios, the *a posteriori* pdf can be computed by an exhaustive search in the model parameter space.

The constant in (4.1) is computed by normalization of the *a posteriori* pdf over the model space. The pdf (4.1) is then represented by the projections of the model points at different probability levels on the planes (strike, dip), (strike, slip), (dip, slip) (Zollo and Bernard, 1991). Each model point is represented by a symbol whose size is proportional to the probability volume it belongs to. Maximum likelihood models can be directly located on the plane projections of the pdf. The extension and the shape of surfaces corresponding to the projected points belonging to a fixed per cent probability level give a measure of parameter resolution and correlation.

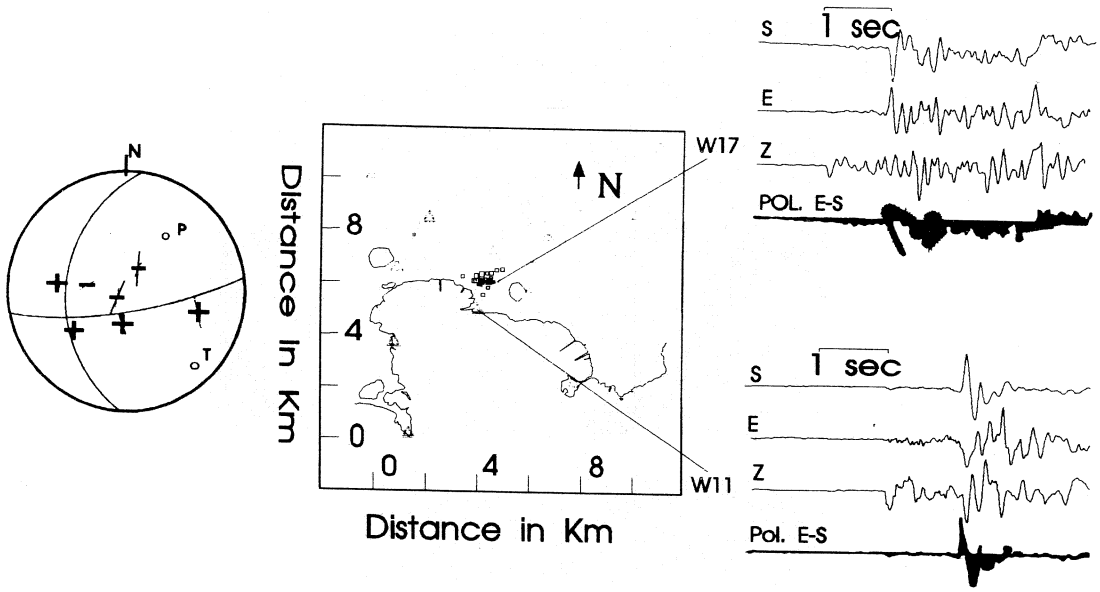

Fig. 3. Campi Flegrei map: epicenter locations (empty squares) of the April 1 swarm. The analyzed earthquake is shown by a filled square. Displacement seismograms (filtered 1-6 Hz) at stations w11 and w17 are displayed, as well as related polarization plots on the right. On the left, is a focal mechanism chosen among the most probable ones for the analyzed earthquake, and consistent with the composite focal mechanism obtained for the whole swarm (see following sessions). *P* wave polarities are displayed, as well as theoretical *S* wave polarizations (gray lines) and measured polarization (thin black lines).

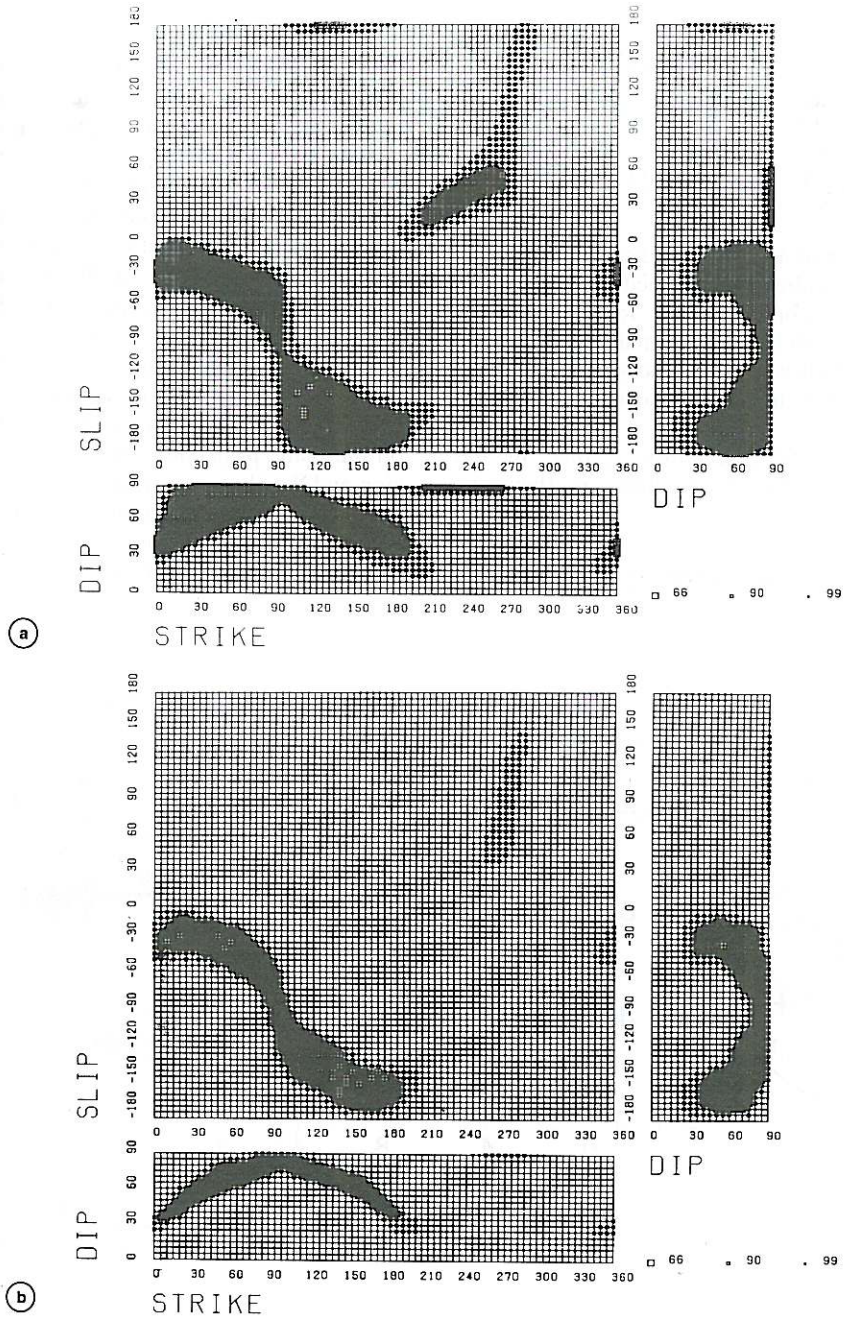

Fig. 4a,b. Probability density projection maps for strike, dip and slip from: a) *P* polarity data; b) *P* polarity data and *S* polarization data. The plots show the projection on the three planes of the parameter space (δ, φ, λ) of the points of the space belonging to levels of probability 0-66% (large square), 66-90% (medium), 90-99% (small).

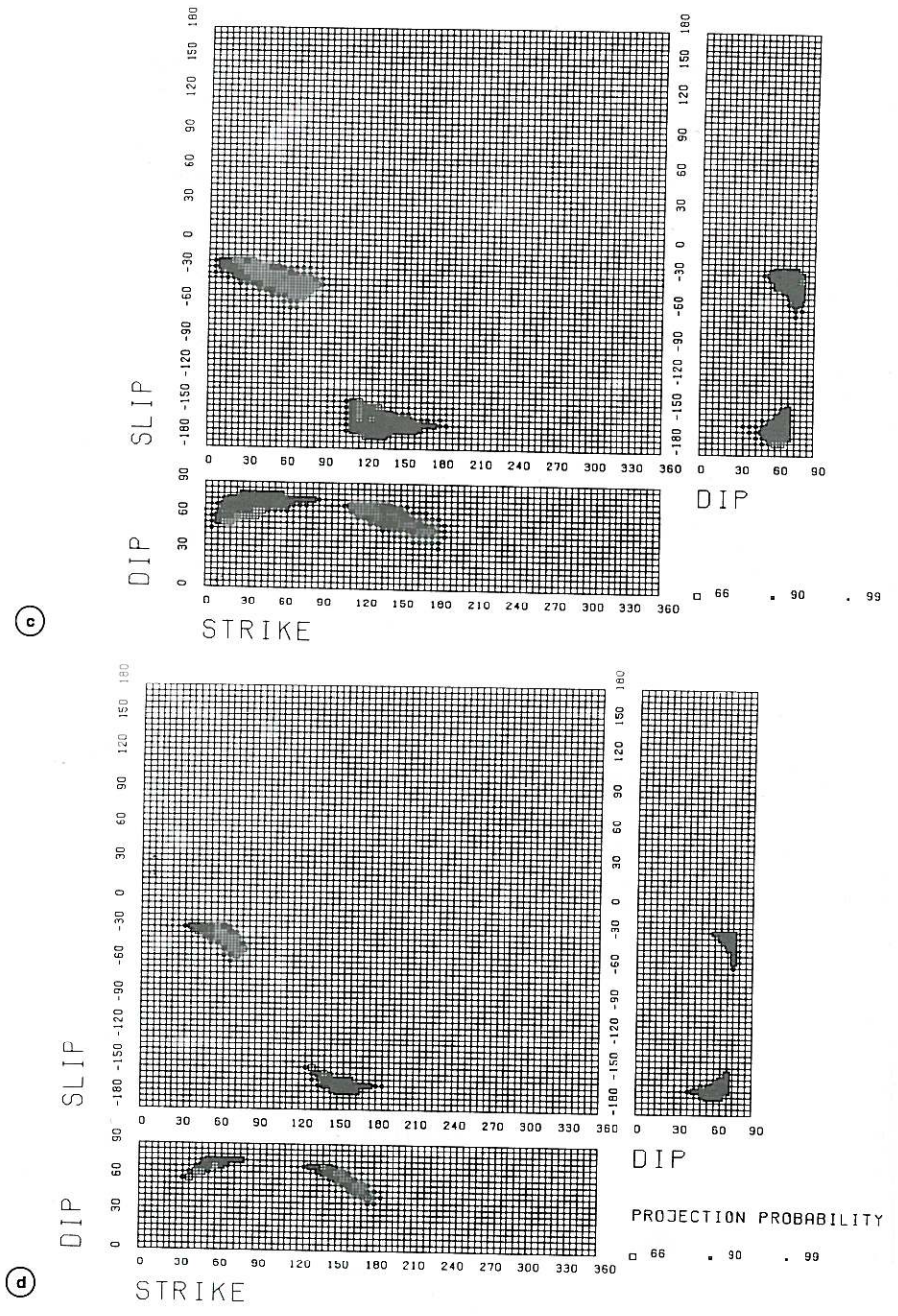

Fig. 4c,d. Probability density projection maps for strike, dip and slip from: c) *P* polarity data and *S/P* amplitude ratios; d) *P* polarity data, *S* polarizations and *S/P* amplitude ratios. The plots show the projection on the three planes of the parameter space (δ, φ, λ) of the points of the space belonging to levels of probability 0-66% (large square), 66-90% (medium), 90-99% (small).

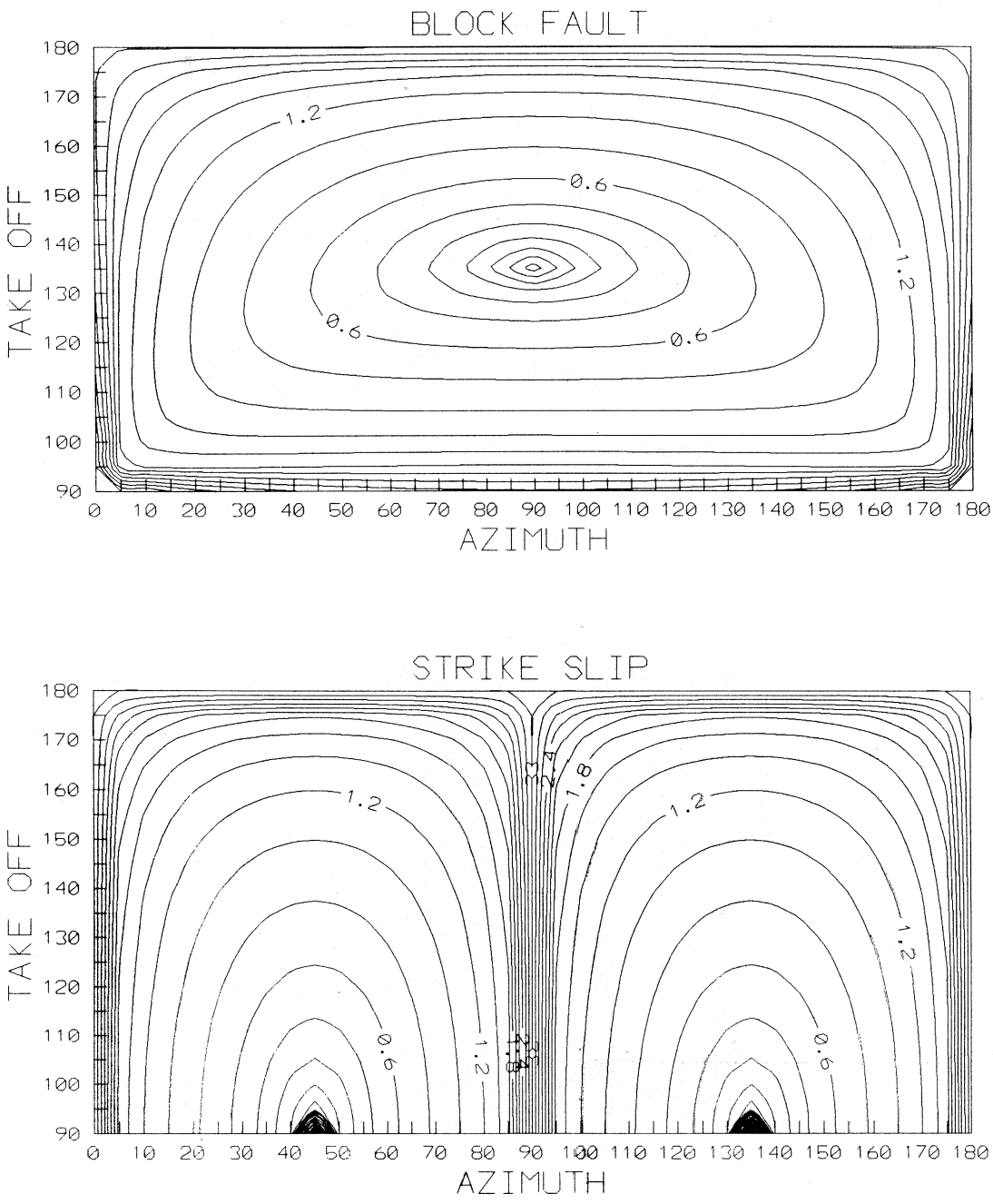

Fig. 5a. Plots showing the logarithm of the *S/P* amplitude ratio as a function of azimuth and take off angles of rays at the source, for different kinds of fault mechanisms: block fault and strike slip. Where the ratio diverges (*P* amplitude equal to 0), saturation values are placed to ± 3 (ratio equal to ± 1000).

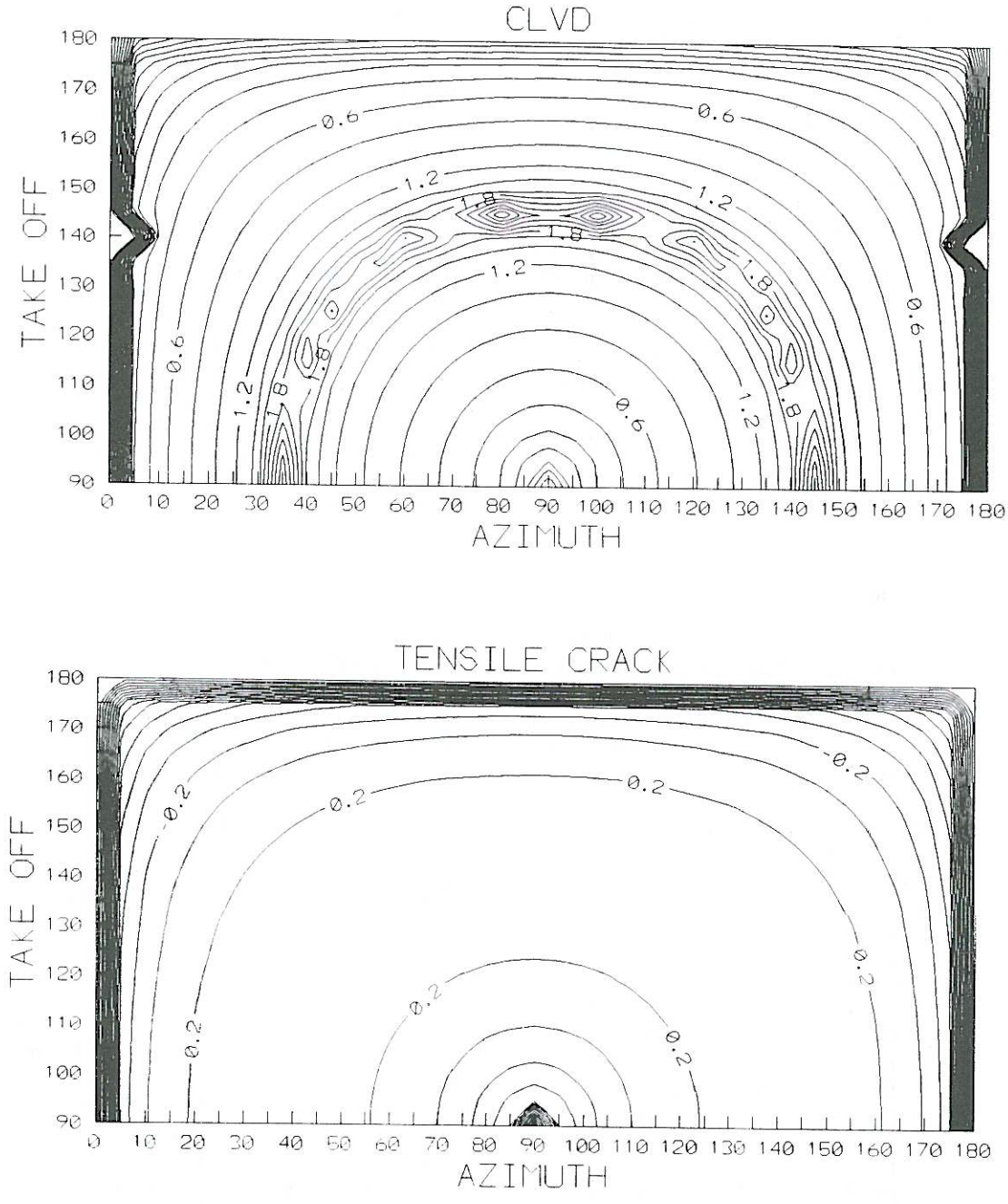

Fig. 5b. Plots showing the logarithm of the *S/P* amplitude ratio as a function of azimuth and take off angles of rays at the source, for different kinds of fault mechanisms: CLVD and tensile crack. Where the ratio diverges (*P* amplitude equal to 0), saturation values are placed to ± 3 (ratio equal to ± 1000).

5. Constraints on focal mechanisms

De Natale *et al.* (1991) show the improvement of the resolution due to the addition of various data sets, for a double couple mechanism.

Figures 3 and 4a-d show this example, obtained for a small (M_L = 2) earthquake occurred at Campi Flegrei caldera on 1984. Parameters for the probability density functions associated with the different data sets are the following:

- for P wave polarities: $\rho_i = \rho = 6$, corresponding to a tolerance of about 10° around the nodal planes; $\gamma_i = \gamma = 0.001$;
- for S polarizations: standard deviation $\sigma_0 = 15°$;
- for S/P amplitude ratios: $\rho_1 = 8$, $a_1 = 5$, $t_1 = 0.5$; $\rho_2 = 11$, $a_2 = 6$, $t_2 = 0.5$.

Tolerance values for the flat part of the pdf for S/P ratios were chosen large enough to include the effect of differential S/P anelastic attenuation, for Q values as low as $Qp = Qs = 50$. Figure 4a shows the probability density distribution on the three fault parameters for a double couple, using the 6 P polarities alone. Figure 4b shows the improvement due to the addition of the 2 S wave polarization directions: the solution is still non-unique. When the two S/P amplitude ratios are added to the P polarities (fig. 4c), the solution appears much more constrained; the three data sets, considered together, finally led to a unique, well constrained solution, as shown in fig. 4d.

The different data sets give variable degrees of constraint on the type of earthquake mechanism. For instance, P onset polarities are not very discriminant among different mechanisms, whereas S/P wave amplitude ratios are strongly sensitive to changes in the type of mechanism. Tensile crack mechanisms are characterized by S/P amplitudes much lower than double couples; CLVD mechanisms are intermediate between the two. Figure 5a,b shows the distribution of S/P amplitude ratios as a function of take off and azimuth angles of the rays, for different source mechanisms: strike slip, block fault, tensile crack and CLVD, for a vertical fault plane oriented N-S. S/P amplitude ratios are strongly variable with the mechanism type; they are less affected by propagation factors than absolute amplitudes, but still affected by differential anelastic attenuation and site effects between P and S waves.

6. Double couple faulting mechanisms of Campi Flegrei earthquakes

The method here described has been applied to the study of microearthquakes which occurred at Campi Flegrei caldera during an episode of strong ground uplift and seismicity (1982-1984). The maximum uplift, at the end of 1984, was of 1.8 m, as measured at the town of Pozzuoli (Berrino *et al.*, 1984). More than 15,000 earthquakes ($0 < Ml < 4.$) occurred during the unrest period, and, on April 1 1984, about 500 earthquakes occurred in 5 hours (Aster *et al.*, 1992). Unrest episodes like this also occurred in 1970-1972 at Campi Flegrei and occasionally in other calderas like Long Valley (USA) (Savage *et al.*, 1987), Yellowstone (USA) (Dzurisin and Yamashita, 1987) and Rabaul (New Guinea) (Mc Kee *et al.*, 1989). The main questions concerning such episodes, called bradyseism from a Greek term, are linked to the mechanism generating ground deformation and seismicity. At Campi Flegrei, ground deformation appeared very concentrated in a small area, almost symmetric around Pozzuoli harbor, which is the center caldera (fig. 6). The very limited extension of the deformed area, which implied a very shallow source for deformation, led De Natale *et al.* (1991) to hypothesize that the mechanism for ground uplift were the heating of shallow aquifers. Other authors hypothesized as source of deformation an intrusion in the form of a shallow (less than 3 km) sill (Dvorak and Berrino, 1991). The main observations at Campi Flegrei, which are common to other calderas, are the high constancy in time of the shape of ground deformation and of the seismic areas (fig. 6). De Natale *et al.* (1993) have recently shown that the joint study of seismic-

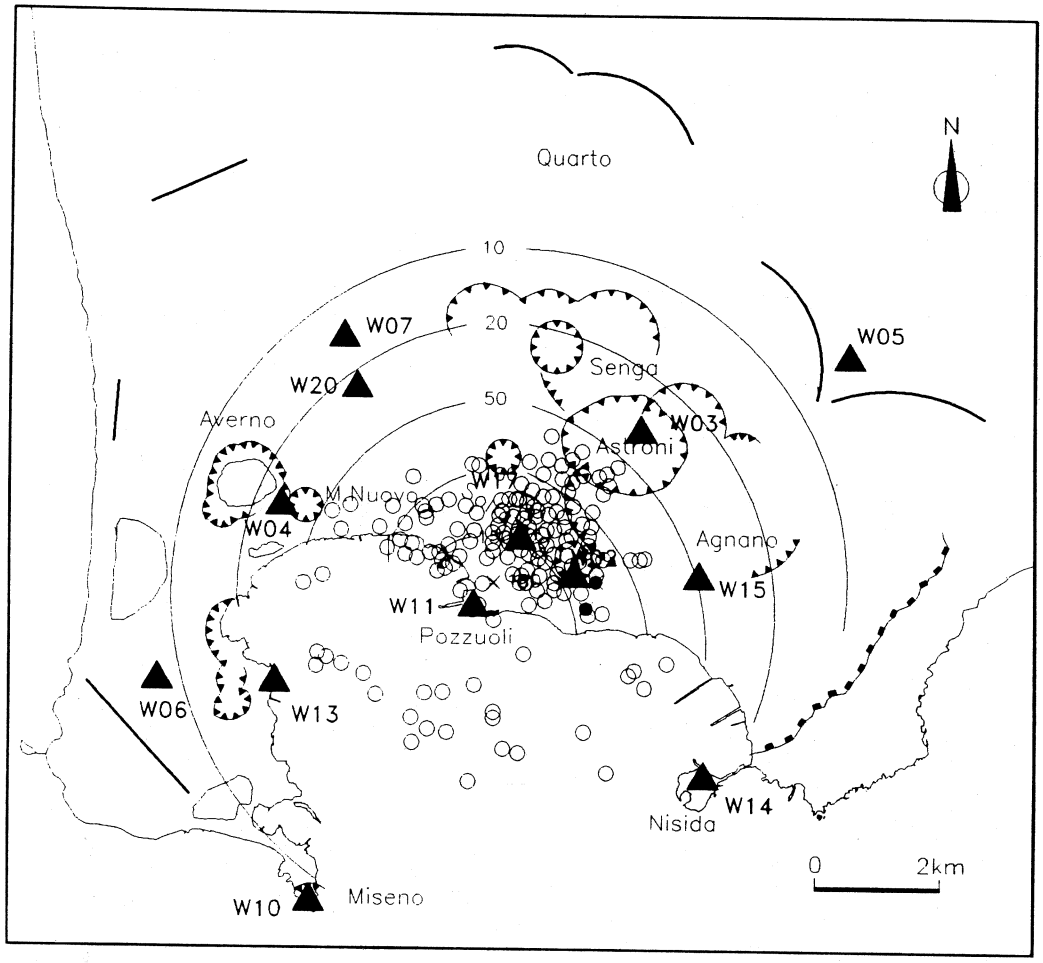

Fig. 6. Campi Flegrei caldera, with the main craters and the geological limits (indicated by black curves). The main configuration of the seismic digital network operated in 1984 is shown by triangles, together with a sample of the seismicity which occurred during the whole 1982-1984 unrest episode. Contours of vertical deformations, showing an almost circular symmetry, are also indicated by thin lines.

ity, ground deformations and gravity anomalies in the area can give a convincing answer to the main volcanological questions.

In the following, I report, as an example of successful study of focal mechanisms for volcanic earthquakes addressed to solving volcanological problems, the focal mechanism study by De Natale *et al.* (1993) on Campi Flegrei earthquakes.

The results will be used to formulate consistent hypotheses on the main geophysical observations performed during unrest episodes.

7. Data analysis

Data are from microearthquakes which occurred at Campi Flegrei during the last unrest

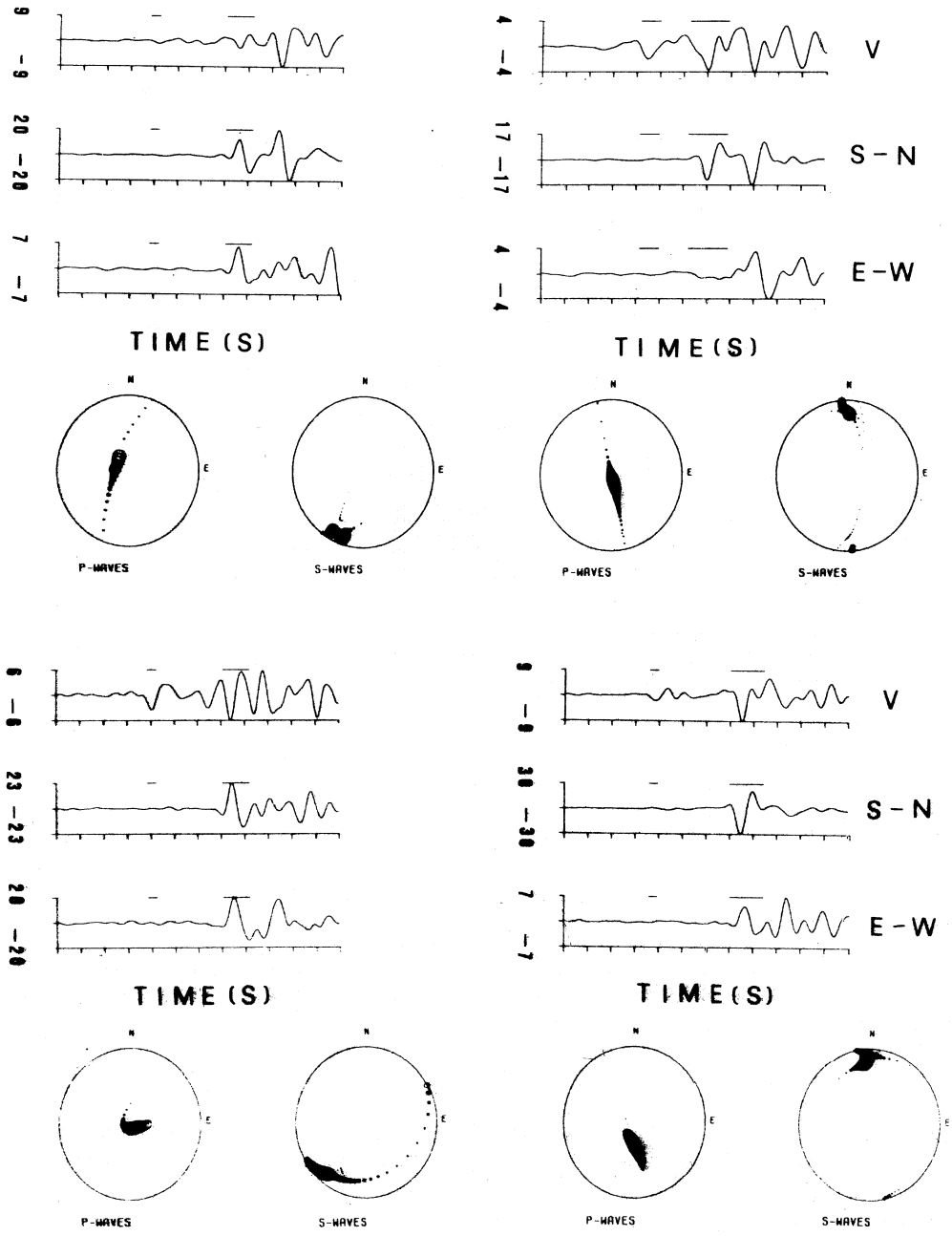

Fig. 7. Some examples of filtered (1.0-6.0 Hz) seismograms and of computation of *P* incidence angles and *S* polarization directions. The parts of seismograms analyzed are marked by bars. On the bottom, the polar diagrams corresponding to the marked parts of seismograms are shown, with amplitude of symbols proportional to the amplitude of the vector in the associated direction.

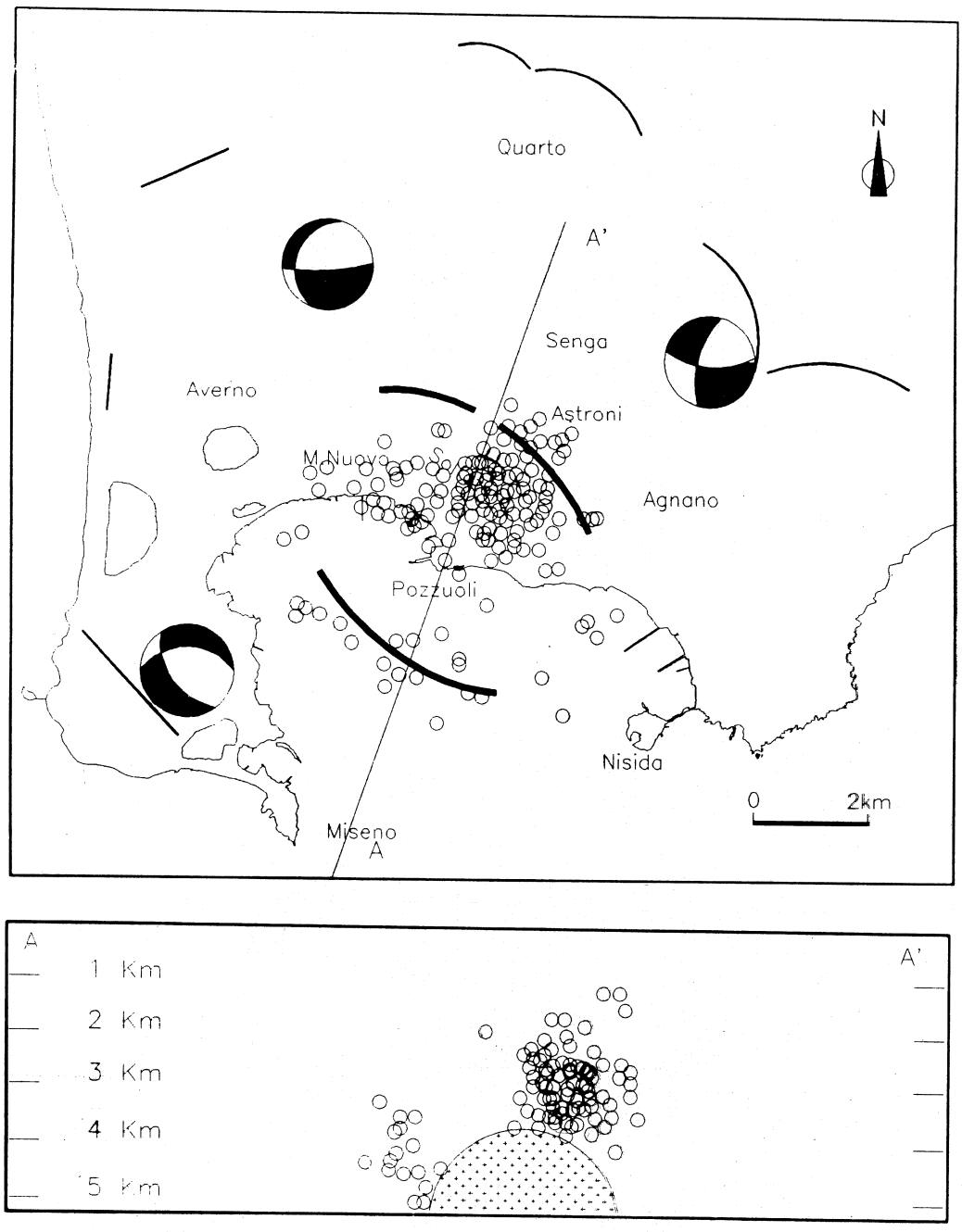

Fig. 8. Earthquake locations and composite focal mechanisms computed for three different areas (swarm, Solfatara, sea). For the April 1 swarm, the mechanism shown was computed using only *P* wave polarities, for all the events.

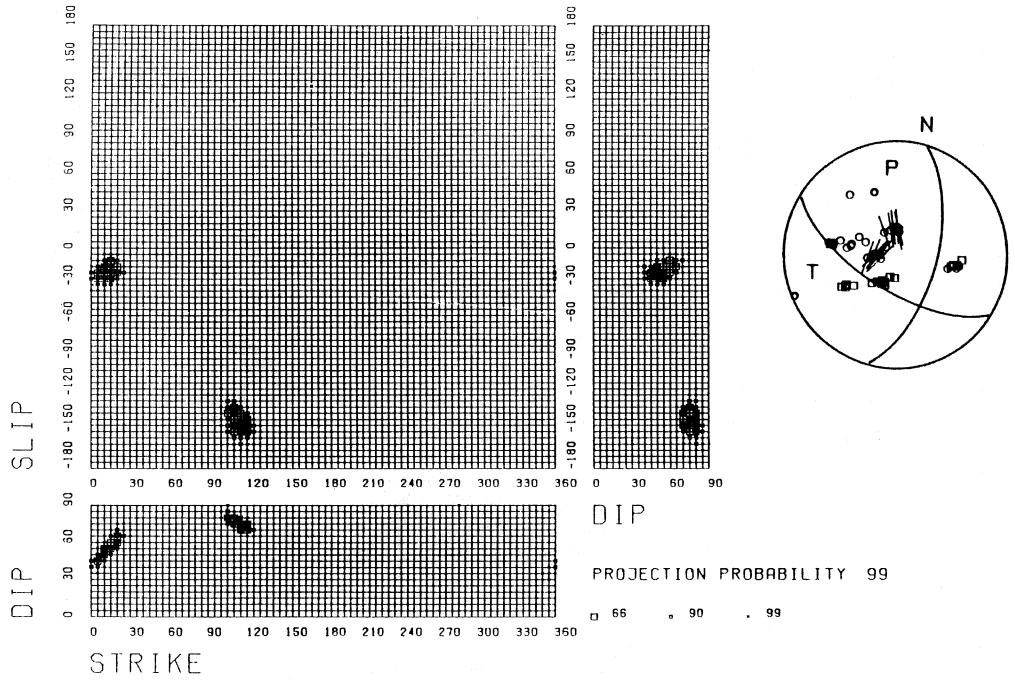
SLIP
DIP
STRIKE
DIP
N
P
T
PROJECTION PROBABILITY 99
66
90
99

(a)

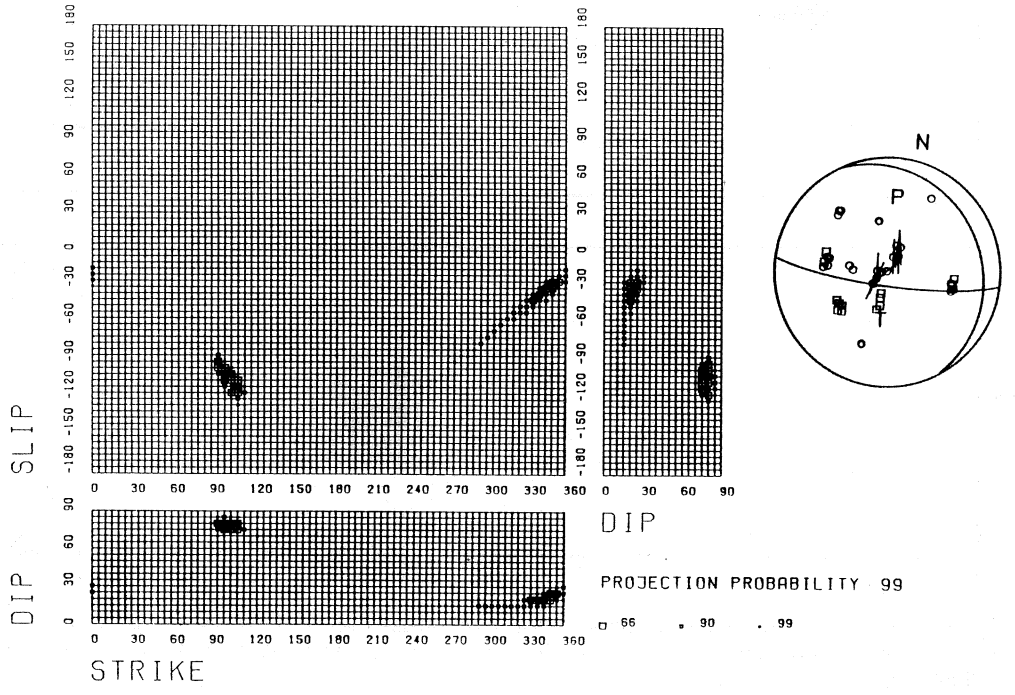
SLIP
DIP
STRIKE
DIP
N
P
PROJECTION PROBABILITY 99
66
90
99

(b)

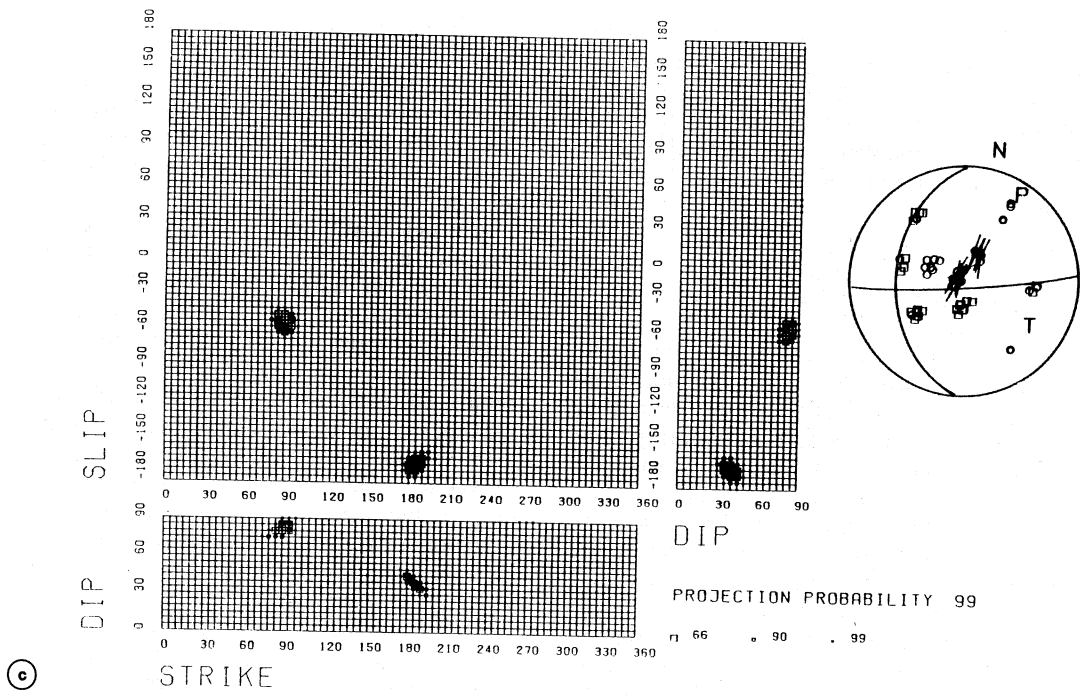

Fig. 9a-c. Probability density distributions computed for three different groups of earthquakes of the April 1 swarm, using *P* polarities and *S* polarizations. The three groups of earthquakes are divided on the basis of the longitude with respect to the Pozzuoli (w11) station: a) NE; b) N; c) NW.

episode (1982-1984) (Aster *et al.*, 1992). On the basis of previous studies by De Natale *et al.* (1987), the source type was assumed as a double couple. *P* wave polarity and *S* wave polarization data were jointly inverted using the described probability method to infer the likelihood of various double couple source models. In particular, 42 earthquakes from the April 1 swarm, ranging in magnitude between 1.0 and 2.5, were analyzed. The values for parameters of probability density distributions were assumed on the basis of location errors, variabilty of the velocity model, and average errors on *S* polarization measurements. On these grounds, values $\rho = 6$, $\gamma = 0.01$ for the probability density function for *P* polarities, and $\sigma = 15°$ for *S* polarizations were assumed (De Natale *et al.*, 1993). Figure 7 shows an example of filtered three component seismograms, used for determination of the *P* wave incidence angle and the *S* polarization direction. The *S* wave incidence angle has been assumed equal to that of the *P* wave, computed by the first phase on three component seismograms. The take-off angles at the source have been computed from ray tracing within three dimensional heterogeneous medium, as obtained from local earthquake tomography by Aster and Meyer (1988). The propagation effect on the observed *S* polarizations has been modeled as only due to the curvature of the ray trajectory, that causes the dip of the polarization plane to change, from a direction perpendicular to the ray at the source to a direction perpendicular to the ray at the receiver, the last one computed from the incidence angle at surface (De Natale *et al.*, 1993).

In addition to the 42 earthquakes belonging to the April 1 swarm, another two groups of earthquakes (fig. 8) have been studied by the

probability method, using only *P* wave polarity data. The first group consists of 13 earthquakes which occurred on land, close to the Solfatara crater, where most of the seismic energy release was concentrated (Aster et al., 1992); the second group consists of 11 earthquakes which occurred at sea.

8. Results and discussion

For the earthquakes which occurred during the April 1 swarm, the analysis of individual mechanisms showed that the *P* axis rotated for events located from east to west with respect to the Pozzuoli station, located at the caldera center. When the earthquakes were divided into three groups, according to their latitude with respect to the caldera center, composite focal mechanisms for each group were very well constrained (fig. 9a-c), and showed a clear rotation of the *P* axis, which is always oriented toward Pozzuoli (fig. 10). This feature was strongly constrained by the *S* polarization direction at the Pozzuoli station, which, for each group of earthquakes showed a very high coherence, within a few degrees (fig. 10). Interestingly, one of the fault planes of each mechanism is always similar to the other ones, and follows the major elongation of the epicenters of the swarm. Figure 8 shows the composite focal mechanisms computed for the events located at the three different zones (swarm, Solfatara, sea), from *P* wave first arrival polarities; for the events of the swarm, the fault plane which is common to the three sub-groups is well represented and, without *S* polarization data, the *P* axis rotation is not seen. As is clear from the figure, earthquake locations and fault planes of the composite mechanisms are consistent with the presence of an elliptical system of inward-dipping fractures. Such fracture system is likely to represent the contact zone between the inner caldera products, mainly composed of loose pyroclastics, and the surrounding rocks.

The collapsed caldera area, filled by light pyroclastics, is well indicated by a negative gravity Bouguer anomaly (Rosi and Sbrana, 1987) shown in fig. 11. The collapsed area, marked by the Bouguer gravity low, is in a good correspondence with the zone enclosed by the elliptical fracture system inferred by seismicity studies, as seen by projecting earthquake hypocenters on the traces of the collapse limits as inferred by modeling of the Bouguer anomaly (fig. 12).

It is noteworthy that all the geophysical evidence is concentrated within a narrow area, about 3 km in radius, coincident with the collapsed caldera area (fig. 12). This area, interestingly, is much smaller (about half the radius) than the larger caldera area as seen from geological evidence. Such discrepancy should indicate that the inner caldera area was formed more recently; however, from the volcanological point of view, there is no clear interpretation on the inner caldera. The most striking volcanological evidence is that all the activity more recent than 5000 years is concentrated within the inner caldera area (Lirer *et al.*, 1987). Thus, it appears that the inner caldera is today the only active part of the Campi Flegrei area. The presence of an innermost, smaller caldera collapse, has been also evidenced for the Rabaul (New Guinea) caldera (Mori and Mc Kee, 1987); also in this case, the seismicity during unrest episodes marks the borders of the inner collapse.

An analysis of the Campi Flegrei earthquakes points out a strict relation between seismicity and ground deformations. The inferred rotation of the compressive axis of focal mechanisms, showing the same radial symmetry of the ground deformations, shows that both seismicity and static deformations are caused by the same stress source. Moreover, the evidence for a lithological discontinuity marking the borders of the inner collapse may have strong implications for the shape and time dependence of the observed ground deformations. As described by De Natale and Pingue (1993), the effect of lateral stress strain discontinuities on the deformations produced by a source of pressure in an elastic medium is to confine the deformation within the area between the discontinuities, and then to make the size of the deformed area almost independent from the source depth.

At Campi Flegrei, as in almost all the

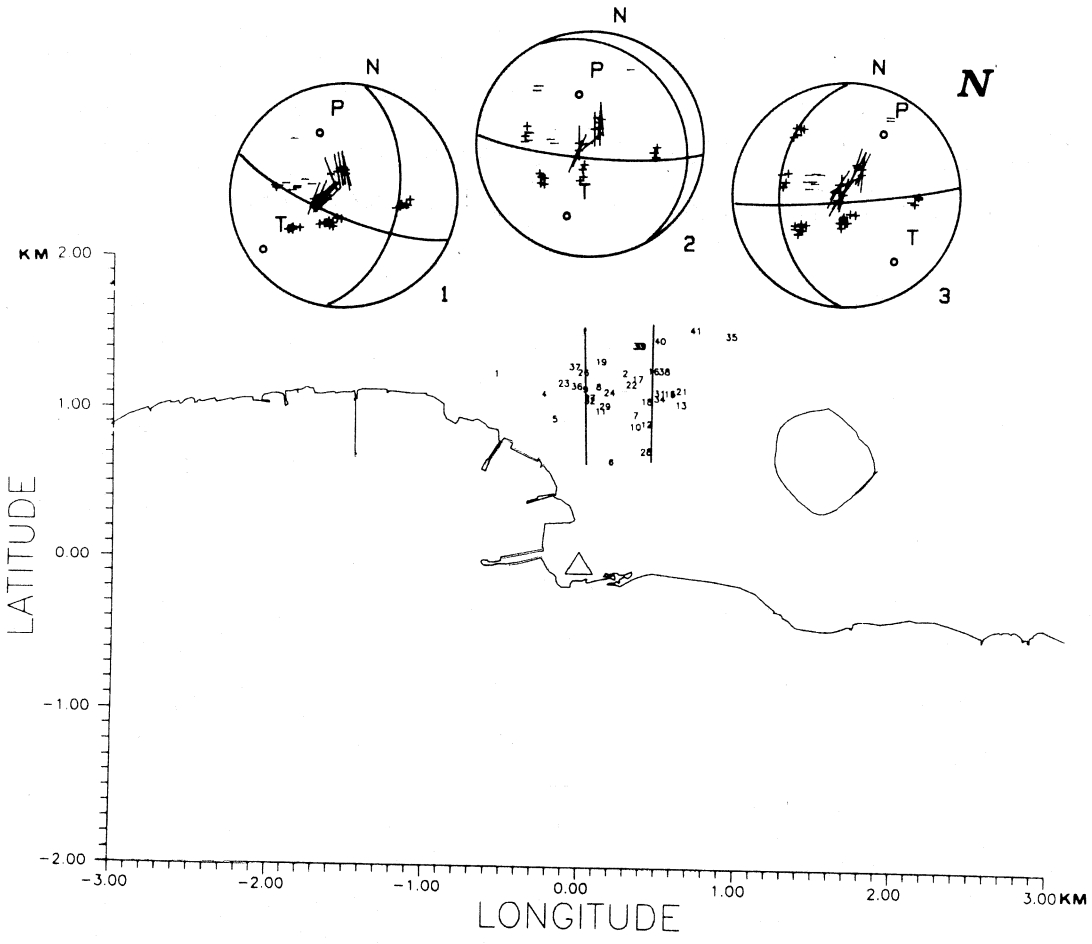

Fig. 10. Highest probability focal mechanisms computed for three groups of the April 1 swarm, plotted on the epicenter map. Different groups of analyzed earthquakes are separated by bars.

calderas, the shape of ground deformations does not change with time. In addition, at Campi Flegrei and Rabaul, ground deformations during unrest episodes involve a very limited area, in such a way that, when interpreted in the framework of a continuous, heterogeneous medium, the inferred depths for the source are very shallow, from 1 to 3 km. If the effect of the caldera border discontinuities is taken into account, the depth of the source may be considerably deeper, producing deformations in a limited area, as observed.

In conclusion, the general picture for the generation of earthquakes at Campi Flegrei during unrest episodes is the following: earthquakes are generated along weakness zones, at the borders of the inner collapsed area, as a response to the change in the stress field responsible for the ground deformations. Ground deformations are also affected by the presence of the stress-strain discontinuities marking the contact between the collapsed area and the surrounding rocks. The effect of such discontinuities is to make the ground deformations con-

centrated in a limited area, with shape not changing with time.

9. Conclusions

The estimation of faulting mechanisms for microearthquakes in volcanic areas is a difficult task, due to the complexity of the medium, and to the need to use robust data able to constrain the solution.

The use of classical methods based on the *P*-wave first arrival polarities is generally not well suited for this problem, because a lot of these data, not easily available in practice, are required to constrain the earthquake mechanisms.

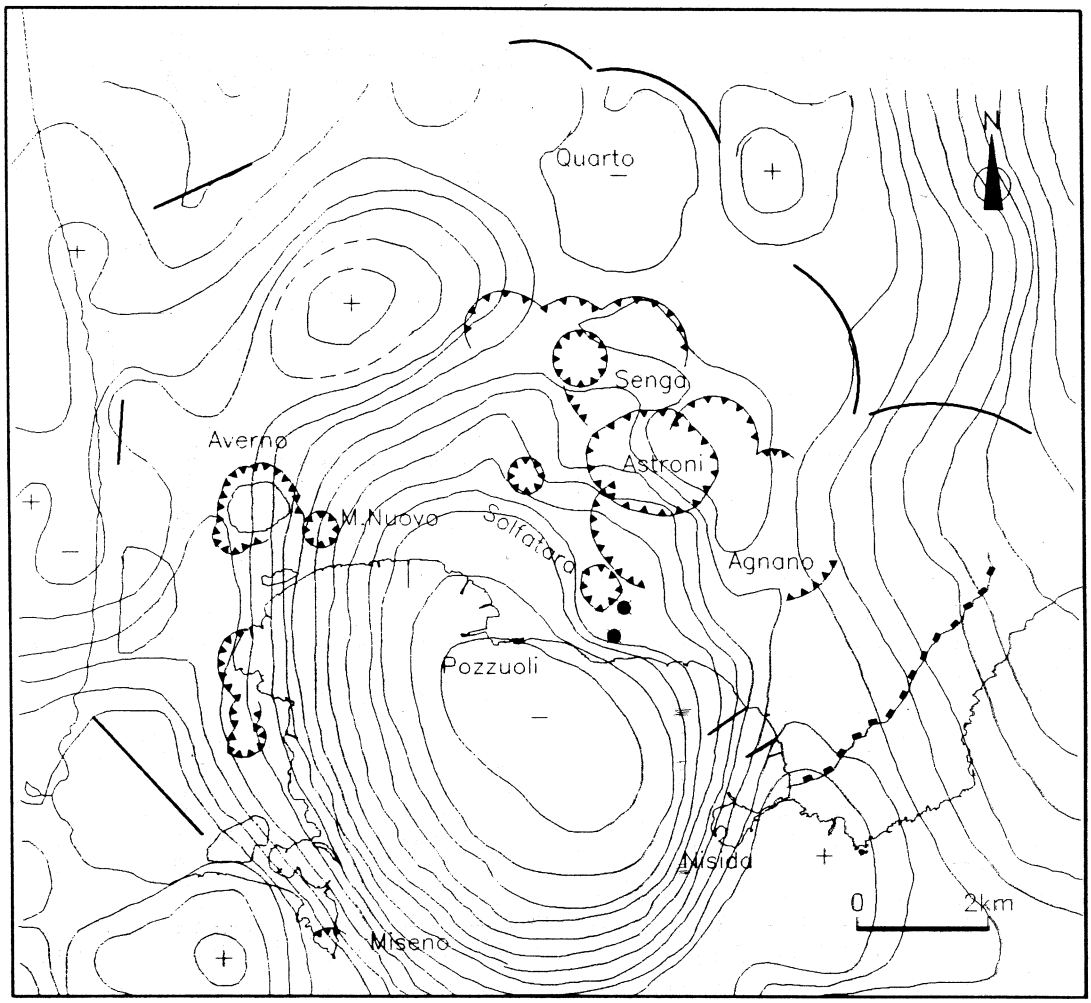

Fig. 11. Bouguer anomaly map at Campi Flegrei caldera (contour interval 1 mgal). Note the sharp minimum, indicating the collapsed caldera area, which is considerably smaller than the area enclosed by geological limits (black heavy lines).

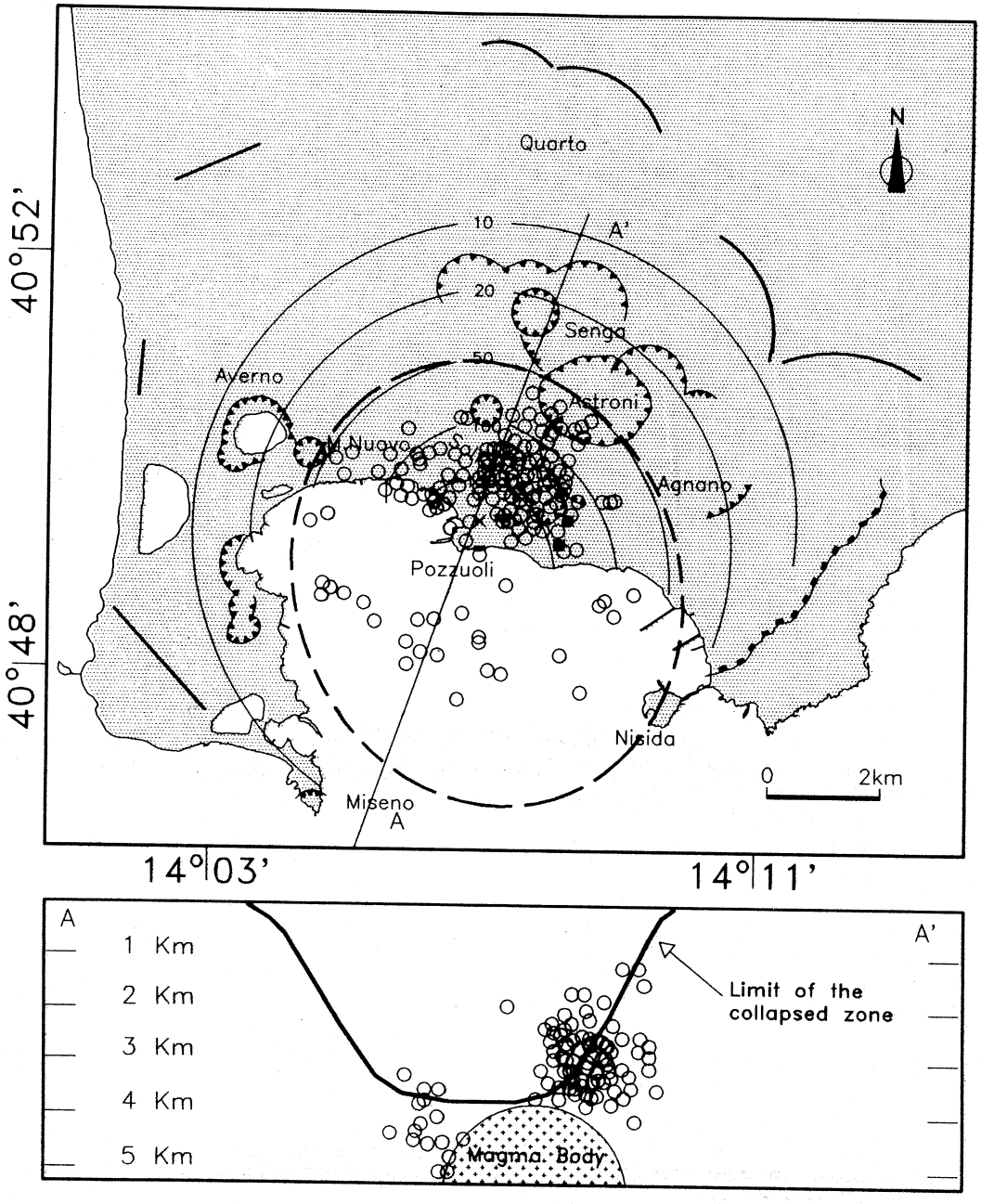

Fig. 12. Sketch of the main geophysical observations at Campi Flegrei caldera. Hatched line indicates the approximate limit of the collapsed area (zero Bouguer anomaly contour). Vertical ground deformations and seismicity are mostly concentrated in this area. Seismicity mainly occurs along the borders of the collapsed area, as indicated in the A-A′ depth section. The approximate location of the magma chamber, as inferred by Ferrucci *et al.* (1992) is also shown (from De Natale *et al.*, 1993).

Moreover, in volcanic areas, it is of great interest to discriminate the kind of mechanism for the earthquakes (double couple, tensile crack, CLVD), not obtainable by *P* polarities alone.

The apparently obvious choice of using absolute *P* and *S*-wave amplitudes to constrain focal mechanisms has a major problem in the marked sensitivity of such data to details of the propagation, for both elastic and anelastic effects.

In particular, details of elastic effects near the recording site, and of anelastic attenuation along the whole propagation path, may strongly bias absolute amplitudes in a way that is very difficult to predict in practice.

The use of robust observables, like the *S* wave polarization directions and, to a lesser extent, the *S/P* amplitude ratios, may help to strongly constrain focal mechanisms of volcanic earthquakes. The *S/P* amplitude ratio, in particular, is very sensitive to the kind of mechanism and is able to discriminate the source type, a very important tool for volcanological purposes.

The best way to use such different observables to study source mechanisms is through a complete analysis of the probability density on the whole parameter space. Such analysis is easily feasible because few (two or three) parameters are able to describe the most common source types.

In order to opportunely manage the different data sets, it is important to use appropriate probability distribution functions. In particular, since *S/P* amplitude ratios are still affected by differential anelastic attenuation and site effects, functions with a large tolerance, able to include unknown effects of this kind, should be used.

The application of a methodology based on these criteria, to microearthquakes which occurred at the volcanic area of Campi Flegrei, has given a coherent picture of unrest episodes in this area. In particular, it has offered new insights into the strict relation between seismicity, ground deformations and caldera structure, which is probably generalisable to other similar calderas.

REFERENCES

Aki, K. and P.G. Richards (1980): *Quantitative seismology: theory and methods* (W.H. Freeman and Co., S. Francisco, CA).

Aster, R.C. and R.P. Meyer (1988): Three-dimensional velocity structure and hypocenter distribution in the Campi Flegrei caldera, Italy, *Tectonophysics*, **149**, 195-218.

Aster, R.C., R.P. Meyer, G. De Natale, A. Zollo, M. Martini, E. Del Pezzo, R. Scarpa and G. Iannaccone (1992): Seismic investigation of the Campi Flegrei Caldera, in *Volcanic seismology*, Proc. Volcanol. Series III (Springer-Verlag, Heidelberg).

Bernard, P. and A. Zollo (1989): Inversion of near source polarization for parameters of double couple point sources, *Bull. Seismol. Soc. Am.*, **79**, 1779-1809.

Berrino, G., G. Corrado, G. Luongo and B. Toro (1984): Ground deformation and gravity changes accompanying the 1982 Pozzuoli uplift, *Bull. Volcanol.*, **47** (2), 187-200.

Brillinger, D.R., A. Udias and B. Bolt (1980): A probability model for regional focal mechanisms, *BSSA*, **70**, 149-170.

Carpenter, E.W. (1966): *Absorption of elastic waves: an operator for a constant Q mechanism*, United Kingdom Atomic Energy AWRE Rep., 0-43/66, 1-16.

De Natale, G., G. Iannaccone, M. Martini and A. Zollo (1987): Seismic sources and attenuation properties at Campi Flegrei volcanic area, *PAGEOPH*, **125** (6), 883-917.

De Natale, G., A. Ferraro and J. Virieux (1991): A probability method for local earthquake focal mechanisms, *Geophys. Res. Lett.*, **18** (4), 613-616.

De Natale, G. and F. Pingue (1993): Ground deformations in collapsed caldera structures, *J. Volcanol. Geotherm. Res.*, **57**, 19-38.

De Natale, G. and A. Zollo (1989): Earthquake focal mechanisms from inversion of *P* and *S* wave motions, in *Digital seismology and fine modeling of the lithosphere*, edited by R. Cassinis, G. Nolet and G. Panza (Plenum Pub. Co.), 399-419.

De Natale, G., A. Ferraro, A. Zollo and J. Virieux (1993): Accurate faulting mechanisms of a 1984 earthquake swarm at Campi Flegrei caldera (Italy), during an unrest episode: implications for volcanological research, *J. Geophys. Res.* (in press).

Dvorak, J., and G. Berrino (1991): Recent ground movement and seismic activity in Campi Flegrei, Southern Italy: episodic growth of a resurgent dome, *J. Geophys. Res.*, **96**, 2309-2324.

Dzurisin, D. and K.M. Yamashita (1987): Vertical surface displacements at Yellowstone caldera, Wyoming, 1976-1986, *J. Geophys. Res.*, **92** (B13), 13753-13766.

Ferrucci, F., A. Hirn, G. De Natale, J. Virieux and L. Mirabile (1992): *P-SV* conversions at a shallow boundary beneath Campi Flegrei Caldera (Italy): evidence for the magma chamber boundaries, *J. Geophys. Res.*, **97** (B11), 15351-15359.

Knopoff, L. and M.J. Randall (1970): The compensate linear vector dipole, *J. Geophys. Res.*, **75**, 4957-4963.

Lirer, L., G. Luongo and R. Scandone (1987): On the vol-

canological evolution of Campi Flegrei, *EOS Trans. Am. Geophys. Union*, **68**, 226-234.

Mc Kee, C, J. Mori and B. Talai (1989): Microgravity changes and ground deformation at Rabaul caldera, 1973-1985, in *Volcanic Hazards*, Proc. Volcanol. Series I (Springer-Verlag, Heidelberg).

Mori, J. and C.O. Mc Kee (1987): Outward-dipping ring-fault structure at Rabaul caldera as shown by earthquake locations, *Science*, **235**, 193-195.

Rosi, M. and A. Sbrana (Editors) (1987): Phlegraean Fields, CNR, *Quad. Ric. Sci.*, **114**, vol. 9, pp. 175.

Savage, J.C., R.S. Cockerham, J.E. Estrem and L.R. Moore (1987): Deformation near the Long Valley Caldera, Eastern California, 1982-1986, *J. Geophys. Res.*, **92** (B3), 2721-2746.

Sileny, J., G.F. Panza and P. Campus (1992): Waveform inversion for point source moment tensor retrieval with variable hypocentral depth and structural model, *Geophys. J. Int.*, **109**, 259-274.

Tarantola, A. and B. Valette (1982): Inverse problems = quest for information, *J. Geophys.*, **50**, 159-170.

Zollo, A. and P. Bernard (1991): Fault mechanism for near source data: joint inversion of *P* polarities and *S* polarizations, *Geophys. J. Int.*, **104**, 441-452.